Title: Distinct place cell dynamics in CA1 and CA3 encode experience in new environments

Authors: Can Dong[1], Antoine D. Madar[1], Mark E. J. Sheffield[1*]

Affiliations:

[1] Department of Neurobiology and Institute for Neuroscience, University of Chicago, Chicago, IL 60637, USA.

[*] Correspondence to: sheffield@uchicago.edu.

Abstract: When exploring new environments animals form spatial memories that are updated with experience and retrieved upon re-exposure to the same environment. The hippocampus is thought to support these memory processes, but how this is achieved by different subnetworks such as CA1 and CA3 remains unclear. To understand how hippocampal spatial representations emerge and evolve during familiarization, we performed 2-photon calcium imaging in mice running in new virtual environments and compared the trial-to-trial dynamics of place cells in CA1 and CA3 over days. We find that place fields in CA1 emerge rapidly but tend to shift backwards from trial-to-trial and remap upon re-exposure to the environment a day later. In contrast, place fields in CA3 emerge gradually but show more stable trial-to-trial and day-to-day dynamics. These results reflect different roles in CA1 and CA3 in spatial memory processing during familiarization to new environments and constrain the potential mechanisms that support them.

22 **Introduction:**

23 The hippocampus plays a critical role in episodic memory by rapidly forming, updating, and
24 retrieving patterns of activity that represent specific memories[1,2]. The CA1 subnetwork is
25 considered the main output of the hippocampus that transmits information to the cortex and
26 other regions[3], but the computational role of CA1 in memory processing remains unclear.
27 Theoretical studies generally highlight networks upstream of CA1, such as CA3 and the medial
28 entorhinal cortex (MEC) as being attractor networks that encode and retrieve representations
29 associated with different environments[3-7]. These representations could then simply be
30 inherited by CA1[8-10]. However, given the many forms of synaptic plasticity at CA1 synapses[11,12],
31 the complex dendritic computations performed by CA1 neurons[13-15] and the diversity of CA1
32 interneurons[16,17], CA1 activity dynamics are unlikely to be purely inherited from upstream
33 regions. Establishing the difference in activity dynamics between CA1 and its inputs will help
34 reveal how information is processed by CA1, which computations are specific to CA1, and what
35 the role of its inputs are.

36

37 Spatial memories are thought to be encoded and retrieved in the hippocampus through the
38 activity of place cells[18-22] – cells with spatially selective firing fields called place fields (PFs). All
39 hippocampal subnetworks (CA1, CA2, CA3, and dentate gyrus) express PFs during
40 navigation[10,18]. Importantly, CA1 pyramidal neurons develop PFs rapidly during exploration of a
41 novel environment[23]. Understanding how hippocampal representations emerge so rapidly
42 during one-shot events is critical to refine theories of memory. However, the specific dynamics
43 and underlying mechanisms of PF emergence in CA1 have only recently come into focus, and

44 even less is known about PF emergence in CA3, the main input region to CA1[11,14,15,24-27]. An
45 important step forward came from analyzing PFs on a trial-to-trial basis during the very first
46 moments in a novel environment[15]. Such trial-to-trial resolution showed that many neurons in
47 CA1 develop a PF on the first trial and engage synaptic plasticity mechanisms in the form of
48 increased dendritic branch spike prevalence[14,15]. Determining the dynamics of PF emergence in
49 CA3 under the same conditions in novel environments will generate new insights into the
50 mechanisms of PF emergence in CA1 and reveal the extent to which CA1 PF emergence is
51 inherited from CA3 PFs.
52
53 In addition to how spatial representations emerge, understanding how they evolve during
54 familiarization to a novel environment (a form of spatial learning) is also critical to refine
55 theories of learning and memory. Little is known about trial-to-trial PF dynamics in CA1 or CA3
56 with most studies focusing on mean PF dynamics across conditions[18,28,29]. In familiar
57 environments it has been shown that PFs in both CA1 and CA3 tend to shift backwards with
58 experience and develop negatively skewed PFs to varying degrees depending on the behavioral
59 paradigm used[29-32]. This is thought to be an experience-dependent process that requires NMDA
60 receptor-dependent long-term synaptic plasticity[33]. How soon these phenomena appear during
61 the familiarization process, and whether they are inherited by CA1 from CA3, remains unclear[31].
62 Tracking large numbers of CA1 and CA3 neurons under the same conditions during
63 familiarization to novel environments will help better understand these phenomena.
64

65 Memory retrieval is thought to be achieved by reinstating the same neuronal activity that
66 occurred during learning[10,34,35]. However, evidence from recordings of large ensembles of place
67 cells have shown that many PFs in CA1 are unstable across exposures to the same familiar
68 environment[13,18,28,36-39]. Again, as with PF emergence and trial-to-trial dynamics, a lot less is
69 known about the stability of CA1 and CA3 PFs during re-exposure to a novel environment. This
70 has left unclear how familiarization influences PF stability. CA1 PFs might be expected to be less
71 stable across days than CA3 PFs as CA1 has been shown to integrate stable spatial information
72 from CA3 with time signals from CA2 upon re-exposures to the same familiar environment[10].
73 Further supporting the idea of reactivation of stable PFs in CA3 comes from its hypothesized
74 role in pattern completion[7], although recent experimental findings tracking PFs in novel
75 environments across days suggest otherwise[18]. Lastly, trial-to-trial retrieval dynamics of single
76 PFs during re-exposure to a novel environment are not known because of the technical
77 difficulty to track the same place cells across days[31]. Overall, how PFs emerge, evolve and
78 stabilize during familiarization to a novel environment is unclear, both in CA1 and CA3.
79
80 In this work we use 2-photon Ca^{2+} imaging to longitudinally record from large populations of
81 CA1 and CA3 pyramidal neurons in head-fixed mice running unidirectionally on a treadmill to
82 repeatedly traverse visually enriched virtual linear environments with consistent behavior. We
83 track neurons from the very first moments in a novel environment and across days to compare
84 the emergence and ongoing dynamics of PFs. We find that PFs initially emerge much faster in
85 CA1 than CA3, but CA1 PFs on average continuously shift backwards with experience. CA3 PFs
86 emerge relatively slowly but are subsequently more reliable than CA1 PFs across trials,

87 displaying less backward shifting. We also find that PF backward shifting decreases with
88 familiarization across trials and across days. Upon re-exposure to the novel environment on the
89 second day, stable PFs in CA3 reactivate rapidly on the first trial, whereas CA1 PFs demonstrate
90 a higher propensity to remap across days. Our findings demonstrate major differences in the
91 initial emergence, shifting, and stability of PFs in CA1 and CA3 during familiarization to a novel
92 environment. The distinct features of CA1 PFs compared to CA3 PFs suggests the CA1 performs
93 significant computations on its spatial inputs from CA3 to support a distinct role in spatial
94 memory processing.

95 **Results**

96

97 **Place field emergence in a novel environment in CA1 and CA3**

98 We expressed GCaMP6f in either dorsal CA1 or CA3a (referred to as CA3 from here on) of
99 different mice (Fig. 1c, d). The Grik4-cre line[40] was used to restrict expression to CA3 pyramidal
100 neurons (Fig. 1c). Importantly, these mice show CRE expression in nearly 100% of pyramidal
101 cells in CA3 which means our recordings were not biased to a sub-population of CA3 pyramidal
102 cells[40]. Using 2-photon microscopy we then recorded calcium transients from pyramidal cell
103 populations in both regions (Supplementary Fig. 1)[13,15]. On experimental day 1 mice were
104 exposed to a familiar (F) environment before being switched to a novel environment (N1) (Fig.
105 1a)[15]. On experimental day 2, mice experienced the same F-to-N switch but to a different N
106 environment (N2; Fig. 1a). N1 and N2 were grouped together and are referred to as N. Mice
107 momentarily slowed down after the transition between environments (Fig. 1b), confirming

108 their perception of the switch to N. Because mice were restricted to running in 1 dimension on
109 a custom-built treadmill, this paradigm led to many repeated traversals in both environments
110 with matched behavior, allowing lap-by-lap PF dynamics to be measured systematically and
111 compared across F and N environments without confounds caused by changes in behavior.

112 As has previously been reported, both CA1 and CA3 place cells globally remapped upon
113 exposure to N (Fig. 2a, b) and displayed altered PF properties compared to F (Supplementary
114 Fig. 2)[4,6,15,18,41-44]. For instance, PF widths were on average larger and PF precision lower in N
115 than F in both CA1 and CA3. Out-of-field PF firing also increased in N versus F as did PF transient
116 occupancy. Crucially, we wanted to observe the real-time emergence dynamics of new place
117 cells in CA1 and CA3 to examine potential differences. Therefore, emergence of new PFs in N
118 was quantified on a lap-by-lap basis (Fig. 2c-e). Some PFs formed instantly, i.e. on the first lap
119 (Instant PFs; Fig. 2c; left), while others were delayed by several laps (Delayed PFs; Fig. 2c; right).
120 Similar to previous observations, many CA1 PFs formed rapidly[14,15,23], with a high proportion of
121 instant PFs (30%; Fig. 2d, e). Unexpectedly, only 9% of CA3 PFs were instant and the distribution
122 of PF onset lap number was more uniform, indicating CA3 PFs form more gradually than CA1
123 PFs (Fig. 2d, e; Supplementary Fig. 2c, d). Supporting this, CA1 place cell activity decoded
124 position on the first lap better than CA3 place cell activity (Fig. 2f-h, Supplementary Fig. 3).
125 These data suggest that in a novel environment, CA1 instantly forms a well-organized map,
126 whereas CA3 forms a map gradually with experience.

127 **Trial-to-trial place field dynamics in a novel environment**

128 To examine and compare how PFs evolve in CA1 and CA3 during spatial learning, we tracked
129 new PFs throughout familiarization to N. We compared the first and second half of the session
130 and found CA3 PFs were more stable than CA1 PFs within a session in N (Fig. 3a). Next, we
131 computed each PF's center of mass (COM) on a lap-to-lap basis (Fig. 3b): in CA1, approximately
132 half of the PFs significantly shifted during the session, but only a third in CA3 (Fig 3c). The
133 direction of shift could go backward or forward relative to the direction of the animal's motion
134 (Fig. 3b-d) but most PFs shifted backwards, with a larger skew in CA1 than CA3 (Fig 3c-d). As a
135 population, CA1 PFs shifted backwards much faster than CA3 PFs (Fig. 3e). This difference is not
136 an artifact of a lower sample size of CA3 PFs as shown by downsampling 1000 times the CA1
137 dataset (Fig. 3e). Removing transients prior to the onset of a robust PF (as we do for defining PF
138 onset lap, see methods) did not alter our conclusions (Supplementary Fig. 4a-b). Individual PF
139 shifting dynamics were not related to PF onset lap or velocity (Supplementary Fig. 5 and 6).
140 Backward and forward shifting PFs occurred at all positions, with large shifts weakly biased
141 towards the end of the track for CA1 (Supplementary Fig. 7).

142 Backward shifting PFs have been previously reported and may be accompanied with an increase
143 in PF width and the development of a negative skew with experience, although reports are
144 conflicting[29-33,45]. We found that, in a novel environment, PF width tended to increase through
145 the first 10 laps in CA1 but not in CA3 (Supplementary Fig. 8). PFs also started with a positive
146 skew that decreased with experience in CA1 but not in CA3 (Supplementary Fig. 8). Note that
147 under calcium imaging, as compared to electrophysiology, PFs are generally positively skewed
148 rather than symmetric as an artifact of calcium transient decay times[46]. An evolution towards
149 less positively skewed and larger PFs suggests that PFs start earlier on the track (see example in

150 Supplementary Fig. 8a), consistent with some electrophysiological reports[32,45]. However,
151 changes in skewness and width were not the only cause of COM backward shifting, as the PFs
152 end position also shifted backwards (Supplementary Fig. 4c-d).

153 Interestingly, we noticed that in CA1 the population tended to shift forward during the first
154 laps, with the global backward shift occurring around the 5th lap (Fig. 3e). We found that the
155 delay in backward shifting was driven by instant PFs that tended to shift forward on early laps
156 (Supplementary Fig. 9). It is worth restating here that CA3 shows few early-onset PFs on the
157 initial laps which is when the forward shifting of instant CA1 PFs occurs. This suggests backward
158 shifting in CA1 might require the presence of established CA3 PFs, which is why instant PFs
159 initially shift forward.

160 **Place field stability upon re-exposure to a novel environment across days in CA1 and CA3**

161 Memory recall of spatial environments is generally thought to be supported by the reactivation
162 of stable PFs upon re-exposures[19-21,47]. We therefore examined the same place cells upon re-
163 exposure to N (specifically N2, see methods) across days (Fig. 4a). On N day 2, increased lap
164 velocity on the first lap compared to the first lap on N day 1 revealed mice had become more
165 familiar with N (Fig. 4b). We then quantified the spatial correlation of mean PFs identified on N
166 day 1 with N day 2, which was on average significantly higher in CA3 (0.70 ± 0.04) than CA1
167 (0.49 ± 0.02) (Fig. 4c-f). The bimodal distribution of CA3 PF spatial correlations (Fig. 4d; bottom)
168 helped categorize PFs as either stable (R > 0.5) or unstable (<= 0.5). In all mice we found that
169 CA3 had a higher fraction of stable PFs compared to CA1 (Fig. 4e). Interestingly, in CA1, we
170 found a small but significant positive correlation between PF shifting on N day 1 and PF spatial

171 correlation across days, suggesting that higher day-to-day PF stability is associated with more
172 stable trial-to-trial PF dynamics upon the first exposure to a novel environment (Supplementary
173 Fig. 10).

174 We then compared the PF onset laps of stable PFs on day 2 (re-emergence, Fig. 4g, left) with
175 PFs that newly formed on day 2, which included both unstable PFs from day 1 (Fig. 4g, middle)
176 and PFs that appeared for the first time on day 2 (Fig. 4g, right). We found that stable PFs re-
177 emerged earlier in the session than newly formed PFs, and this difference was much more
178 apparent in CA3 than CA1 (Fig. 4h, right). Further, a high proportion of CA1 PFs are continuously
179 forming even as the environment becomes familiar. Lastly, similar to day 1, the vast majority of
180 new PFs in CA3 emerge gradually after a delay with very few instant PFs (Fig. 4h, bottom-middle
181 and bottom-right) whereas the CA1 again shows a much higher proportion of instant PFs on day
182 2 (Fig. 4h, top-middle and top-right). This reveals that stable CA3 PFs are retrieved much faster
183 than new PFs emerge during re-exposure on day 2, whereas stable and new PFs in CA1 show
184 similar emergence dynamics.

185 **Lap-by-lap dynamics across days**

186 We first asked if there was any evidence of continuous PF shifting of the population occurring
187 offline between sessions separated by a day. We found no such evidence as the distribution of
188 PF shift distance between the end of the session on day 1 and the start of the session on day 2
189 was not skewed (Fig. 5a). This indicates that COM shifting reflects experience-dependent
190 processes that occur during ongoing familiarization but do not continue offline. However, when
191 considering only stable PFs that on day 1 showed statistically significant backward shifting, we

192 found they tended to reset on day 2 toward their original position on the early laps of day 1
193 (Fig. 5b, Supplementary Fig. 11). Therefore, although shifting does not continue offline, offline
194 processes may be involved in resetting PFs back towards their original position.

195 We then asked whether the PF shifting dynamics we had observed on day 1 in N continued
196 upon re-exposure on day 2. The few stable PFs that exhibited significant shifting on both days
197 did not change much on average, but the direction and amplitude of individual PF shifts were
198 not correlated across days (Fig. 5c). At the population level, which was thus mostly driven by
199 newly shifting PFs, we found that CA1 PFs on average shifted backwards like on day 1, before
200 stabilizing after lap 15 (Fig. 5d). The CA3 map shifted less than CA1 (Fig. 5d, right). In contrast to
201 day 1, we observed a decrease in PF width over the first laps in CA1, but not CA3, and little
202 change in skewness with population dynamics indistinguishable between CA1 and CA3
203 (Supplementary Fig. 8).

204 Formally comparing dynamics on N day 1, N day 2 and very familiar environments (F), we found
205 that CA1 population backward shifting slowed down and stabilized with familiarization across
206 days (Fig. 6a, c). Stabilization also tended to occur earlier with the level of familiarity: in
207 contrast to day 1, a plateau was reached on day 2 after 15 laps, and only after 12 laps in F.
208 Shifting of the CA3 map showed a similar trend than CA1 although changes with familiarization
209 across days were less obvious (Fig. 6b, d), in part because shifting dynamics were already slow
210 on day 1. Resampling the CA3 data revealed extensive overlap in the population shift across
211 conditions, indicating similar dynamics, (Fig. 6d, right). This analysis also revealed that the
212 population becomes more homogeneous with familiarization across days (smaller variance in

the slope distribution). Finally, in CA1, PF skewness and width tended to evolve and stabilize with familiarization, whereas the CA3 population did not show clear dynamics despite homogenizing across days (Supplementary Fig. 8). These results suggest that lap-wise PF dynamics are enhanced by novelty and decrease as a function of familiarity in CA1, and these PF changes are less apparent in CA3.

Discussion

We used 2-photon calcium imaging of large populations of dorsal CA1 and CA3 pyramidal neurons to measure and compare the emergence, shifting dynamics, and longitudinal stability of PFs in novel environments with trial-to-trial resolution. We found that PFs emerge faster in CA1 but place cells are constantly renewed across exposures whereas they emerge later in CA3 with less turnover across exposures. After emergence, the location of the PFs is not always stable, sometimes showing prominent backward or forward shifting from lap-to-lap. The average spatial representation in the hippocampus shifts backwards, with a faster shift in CA1 than CA3. This backward shifting slows down with familiarization across days. These findings support the idea that CA3 and CA1 perform distinct functions during familiarization to a novel environment, and CA1 does not simply inherit spatial information from CA3 during this form of spatial learning. They also constrain the potential mechanisms explaining how spatial representations emerge, evolve, and reactivate in the hippocampus.

234 Consistent with previous reports, we observed hippocampal PFs that emerged instantly in a
235 novel environment (on the very first trial) and others that emerged after multiple trials (delayed
236 onset PFs)[14,15,23]. Interestingly, the proportion of instant PFs was much lower in CA3 than CA1
237 (Fig 2). Although to our knowledge this is the first time the trial-to-trial emergence of CA3 PFs
238 has been reported in completely novel environments, a related study did compare the
239 emergence of PFs in CA3 and CA1 in a familiar linear belt with novel sensory cues added[29]. This
240 study found 2 types of place cells: 1) landmark vector (LV) cells that have multiple instant PFs
241 locked to sensory cues and 2) place cells with single PFs with a mix of instant and delayed-onset
242 PFs that emerge when novel sensory cues are added. Interestingly, they found 10 times more
243 LV cells in CA1 than CA3. Because PFs in LV cells emerged instantly, the larger proportion of LV
244 cells in CA1 is consistent with our finding that CA1 has more instant PFs than CA3. We
245 confirmed that CA1 has a lot more place cells with multiple PFs than CA3 (10-15% in N and F in
246 CA1 vs 1-2% in CA3), but, in contrast to LV cells, only a fraction of them had instant PFs (31% in
247 CA1 in N, comparable to the 27% instant PFs of single-PF place cells). There was no difference
248 between multi- and single-PF place cells in the distribution of onset laps (2-sample KS-test p =
249 0.4 in N, CA1). This might be due to differences in paradigms. For instance, in contrast to the
250 global remapping and emergence of PFs distributed across the whole track that we see in new
251 environments, adding a cue to a familiar environment only induces partial remapping and PF
252 emergence near cues[29].
253
254 Rapid PF emergence in a novel environment in CA1 is thought to rely on a combination of
255 strong, spatially tuned excitatory inputs that do not need to be potentiated[14] and high neuronal

256 excitability, either from novelty-induced disinhibition[16] or from intrinsic properties (low firing
257 threshold, bursting propensity)[26]. CA3 is the main source of excitatory inputs to CA1 and is
258 known to drive CA1 spatial representations in a majority of neurons, at least in familiar
259 environments[48]. It was thus surprising to find that instant PFs were much less prevalent in CA3
260 than CA1 (Fig 2). The simplest explanation is that CA1 instant PFs are not inherited from CA3
261 inputs during initial exploration. Indeed, not all CA1 place cells are necessarily driven by CA3[48]
262 as CA1 receives other sources of spatially modulated inputs (entorhinal cortex[4], CA2[10], non-
263 imaged subareas of CA3[49] , nucleus reuniens[50]), but the emergence dynamics of spatial
264 representations in these areas are not currently known. Alternatively, CA1 instant PFs could be
265 driven by the few CA3 neurons with instant PFs if those neurons have a high degree of
266 divergence to CA1. Low dendritic inhibition in CA1 pyramidal cells upon initial exposure to novel
267 environments could serve to amplify the low number of CA3 inputs[15,25,51]. Delayed onset CA3
268 neurons as well as neurons with unstable spatial modulation could also partially contribute to
269 CA1 instant PFs since some of them are active on early trials.
270
271 After PF emergence, PF properties (position, width, shape) evolve with familiarization and their
272 dynamics have been used as a proxy to study the synaptic plasticity mechanisms supporting
273 spatial representations in the hippocampus[30,32,45]. Initial reports showed that, in a familiar
274 environment, the population of CA1 PFs shifts backwards with experience, a phenomenon
275 consistent with Hebbian rules[32,45] and dependent on NMDA-receptors[33]. Later
276 electrophysiological studies compared lap-by-lap shifting dynamics in CA1 versus CA3 under
277 different familiarity levels[29-31]. Despite discrepancies across studies attributable to different

278 ways of defining novelty, our results are generally consistent with these studies, especially with
279 Roth et. al. (2012)[31] who used completely new distal and proximal cues. We observed
280 significant backward shifting of the population of PFs on day 1 of a new virtual environment in
281 CA1, and to a lesser extent CA3, with the shift slowing down with familiarization across days
282 (Figs. 3, 5, 6). Consistent with most reports[31,32,45], we found that CA1 was still backward shifting
283 in very familiar environments, but not CA3 (Fig. 6).
284
285 Population backward shifting was initially reported to coincide with increased negative
286 skewness and enlargement of PFs[32,45]. However, in contrast to backward shifting, skewness and
287 width dynamics are inconsistent across studies[30,31], suggesting a heterogeneity of mechanisms
288 leading to backward shifting[30,52]. Our data indicates that population backward shifting in CA1 in
289 a novel environment is due to a combination of PF expansion, skewness changes and pure
290 translation of the PF (Supplementary Figs. 4, 8). These dynamics were dependent on familiarity,
291 with changes in skewness closely matching population backward shifting. We did not detect
292 clear dynamics in PF width or skewness in CA3, revealing a dissociation in mechanisms
293 supporting population shifting between CA3 and CA1.
294
295 In addition to the population trend, we characterized shifting dynamics in individual PFs,
296 revealing that half of PFs show significant linear shifts in CA1, mostly backward, compared to
297 only a third in CA3 (Fig. 3c). PFs with large shifts tended to be less stable across days
298 (Supplementary Fig. 10), suggesting that the same mechanisms may underly lap-by-lap and day-
299 to-day stability. On the other hand, PFs that significantly shifted on N day 1 but were stable

300 across days tended, upon re-exposure on day 2, to reset their location toward their original
301 position on day 1 (Fig 5b, Supplementary Fig. 11). This reset opposite of the direction of shifting
302 shows that the plasticity underlying lap-by-lap shifting does not continue offline and is thus
303 experience-dependent[32]. It also shows that lap-by-lap plasticity does not necessarily cause long-
304 term changes in PFs. Together, these findings suggest that the effects of weak lap-by-lap
305 plasticity decay offline (resetting PFs across exposures), whereas strong lap-by-lap plasticity
306 promotes remapping across sessions.
307
308 Interestingly, we found that PFs did not shift backward in CA1 for the first few trials in the novel
309 environment, they actually shifted forward on average (Supplementary Fig. 9). This fits with the
310 idea that synapses from CA3 place cells could be necessary to initiate backward shifting in CA1,
311 as only a very small number of CA3 PFs emerge on initial laps in the novel environment. As
312 more CA3 PFs emerge those synapses may undergo asymmetric plasticity, such as spike-timing-
313 dependent plasticity (STDP)[12] and behavioral time-scale plasticity (BTSP)[11,24], which could start
314 backward shifting in CA1[11,30-33]. Indeed, both STDP and BTSP are known to occur at CA3-CA1
315 synapses of pyramidal neurons[11,12,24] but other synapses could also be involved.
316
317 A classic STDP rule fits well with the extent of backward shifting we observe across laps[32,52] as it
318 can potentiate synapses activated up to 20 milliseconds prior to postsynaptic firing, which,
319 based on the average running speed we observed, would maximally shift PFs backwards by ~0.5
320 cm/lap, approximately what we see in CA1 on N day 1. However, STDP is not always
321 asymmetric at CA3-CA1 synapses, depending on induction protocols[12]. Moreover, the relevance

322 of this type of time-dependent plasticity *in vivo* has been called into question as synaptic
323 changes might just be too weak to yield an effect on single trials[53,54]. On the other hand, BTSP
324 induces larger synaptic changes[24] and may thus be more likely to produce visible shifting effects
325 over single trials. However, BTSP requires plateau potentials associated with burst firing, and
326 those may not happen on most laps[24,55,56], which is likely necessary to see continuous linear
327 shifts like we observed. BTSP can also lead to potentiation of synapses activated several
328 seconds prior to burst firing, which could induce larger PF shifting than observed here. In
329 addition, BTSP has only been found at CA3-CA1 synapses so far and may not occur in CA3
330 pyramidal neurons even though CA3 shows some backward shifting, albeit less than CA1. Lastly,
331 there is evidence that cholinergic input from the medial septum could play a role in regulating
332 backward shifting, at least in CA1[57]. It is therefore not yet clear which mechanisms are driving
333 backward shifting in CA1 and CA3 place cells. The mechanisms supporting forward shifting in
334 some neurons is also unknown. Our careful characterization of the shifting phenomenon in
335 both CA1 and CA3 will constrain future computational models to clarify how hippocampal
336 physiology supports plasticity of spatial representations.
337
338 The reinstatement of the same place code upon re-exposure to the same environment is
339 generally thought to provide a neural substrate for remembering the environment[19-21,47]. Single
340 unit recordings supported this idea by showing place cells remain stable over long
341 periods[58]. However, recent evidence from calcium imaging of large ensembles of place cells has
342 shown that many place cells in CA1 are unstable across exposures to the same
343 environment[10,13,18,28,36-39]. Rather than a deterioration in the memory representation of the

environment, such remapping may serve a function and has been proposed to encode distinct episodes that occur in the same environment separated by time or small changes in environment[10,37,39,41,59-63]. This remapping might therefore allow the animal to create independent representations of different episodes associated with the same environment and favor mnemonic discrimination of those episodes[64,65]. Our data support this idea as the average PF correlation in CA1 across days in a novel environment was 0.49 ± 0.02 (see methods) revealing considerable remapping across days (Fig. 4). This value is higher than what is reported in a recent study using methods similar to ours (~0.2)[18]. This discrepancy could come from differences in environment complexity which has been shown to influence PF stability and reliability[18,66], although no differences were observed between moderate and enriched visual environments, only impoverished environments showed reduced stability[18]. Differences in the experimental paradigm could also factor in: they switched repeatedly back and forth between novel and familiar environments within a single recording session, whereas our mice switched only once, defining only two different episodes (familiar and novel). Increased remapping due to repetitive switching, which defines several episodes, is consistent with the hypothesis of CA1 tracking distinct episodes.

A constantly changing place code in the hippocampus could nevertheless be problematic as information about the familiarity of the environment would be lost. CA3 has long been theorized to have a stable code to support memory recall through pattern completion via recurrent connections[7]. We show that CA3 place cells are indeed more stable across exposures to a novel environment than CA1 place cells. To our knowledge the only other study to track

366 CA3 place cells across days in a *novel* environment did not observe higher stability in CA3 (~0.1
367 spatial correlation in their study versus ~0.7 reported in Fig 4)[18]. In addition to differences of
368 task design stated above, this discrepancy could be explained by their inability to distinguish
369 between CA3 and CA2 cells, as CA2 cells are known to have unstable place coding properties[10].
370 Another related study did find a similar effect as we report here in familiar environments[39] and
371 concluded that CA3 provides a highly stable representation of space and context but little
372 information about time, whereas CA1 is selectively required to integrate CA3 spatial/contextual
373 and CA2 temporal information over hours and days. We add to this framework by showing that
374 the reactivation of stable place cells in CA3 occurs rapidly (on the first traversal) upon re-
375 exposure to the environment. This is consistent with the idea of the CA3 recurrent connectivity
376 being the support of pattern completion through discrete attractors, CA3 activity rapidly
377 settling in the correct attractor basin upon re-exposure[5]. Transition dynamics from one
378 attractor to the next likely depend on specific connectivity and excitability properties:
379 identifying the characteristics of recurrent neural network models that would fit the fast
380 transition we observed will be essential to understand the elusive mechanisms of hippocampal
381 remapping.
382
383 Overall, the differences in emergence, shifting, and stability of PFs in CA1 and CA3 suggest
384 distinct roles and mechanisms at play in these hippocampal subnetworks to support spatial
385 memories. Instant CA1 PFs could mediate the ability of the hippocampus to rapidly represent
386 episodes on a single trial, a feature of episodic memory[67]. The backward shifting of the PF
387 population during ongoing experience could allow CA1 to gradually better predict future

388 locations within an environment before physically arriving at those locations[11,68,69]. CA1,
389 therefore, rapidly generates unique representations of the world that are then continuously
390 updated by exploratory experience to predict the near future (where am I going?). In parallel,
391 the CA3 gradually forms representations with stable trial-to-trial dynamics, thus encoding
392 location in the present moment (where am I currently?). This function seemingly extends across
393 time as relatively stable CA3 spatial representations are rapidly reinstated upon re-exposure to
394 the same environment, possibly to support memory recall through pattern completion.
395 Remapping of CA1 spatial representations across days may instead serve to separate events
396 occurring in the same environment into distinct memory episodes[70]. This framework is depicted
397 in a conceptual model in Supplementary Fig. 12.
398

399 **Acknowledgments:** We thank D. Dombeck for comments on the manuscript, C. Cherian for
400 helpful manuscript edits, and members of Sheffield lab for manuscript comments and useful
401 discussions. **Funding:** This work was supported by: The Whitehall Foundation, The Searle
402 Scholars Program, The Sloan Foundation, The University of Chicago Grossman Institute for
403 Neuroscience start-up funds, and the NIH (1DP2NS111657-01). **Author contributions (CRediT):**
404 Conceptualization: MS, Data curation: CD, Formal Analysis: CD, AM, MS, Funding acquisition:
405 MS, Investigation: CD, Methodology: MS, CD, AM, Project administration: CD, Software: CD
406 Supervision: MS, AM, Validation: AM, MS, Visualization: CD, AM, MS, Writing – original draft:
407 MS, CD, Writing – review & editing: AM, MS, CD.
408 **Competing interests:** Authors declare no competing interests

Data and materials availability: Scripts used for data analysis are available on GitHub public repository (https://github.com/Candong/Distinct_CA1_CA3.git). The raw imaging data are available from the corresponding author upon reasonable request. Source data for each figure are provided with this paper.

References:

1 Parisi, G. I., Kemker, R., Part, J. L., Kanan, C. & Wermter, S. Continual lifelong learning with neural networks: A review. *Neural Netw* **113**, 54-71, doi:10.1016/j.neunet.2019.01.012 (2019).

2 Kitamura, T. *et al.* Engrams and circuits crucial for systems consolidation of a memory. *Science* **356**, 73-78, doi:10.1126/science.aam6808 (2017).

3 Goode, T. D., Tanaka, K. Z., Sahay, A. & McHugh, T. J. An Integrated Index: Engrams, Place Cells, and Hippocampal Memory. *Neuron* **107**, 805-820, doi:10.1016/j.neuron.2020.07.011 (2020).

4 Latuske, P., Kornienko, O., Kohler, L. & Allen, K. Hippocampal Remapping and Its Entorhinal Origin. *Front Behav Neurosci* **11**, 253, doi:10.3389/fnbeh.2017.00253 (2017).

5 Knierim, J. J. & Zhang, K. Attractor dynamics of spatially correlated neural activity in the limbic system. *Annu Rev Neurosci* **35**, 267-285, doi:10.1146/annurev-neuro-062111-150351 (2012).

6 Jeffery, K. J. Place cells, grid cells, attractors, and remapping. *Neural Plast* **2011**, 182602, doi:10.1155/2011/182602 (2011).

7 Kesner, R. P. & Rolls, E. T. A computational theory of hippocampal function, and tests of the theory: new developments. *Neurosci Biobehav Rev* **48**, 92-147, doi:10.1016/j.neubiorev.2014.11.009 (2015).

8 Solstad, T., Moser, E. I. & Einevoll, G. T. From grid cells to place cells: a mathematical model. *Hippocampus* **16**, 1026-1031, doi:10.1002/hipo.20244 (2006).

9 Neher, T., Azizi, A. H. & Cheng, S. From grid cells to place cells with realistic field sizes. *PLoS One* **12**, e0181618, doi:10.1371/journal.pone.0181618 (2017).

10 Mankin, E. A., Diehl, G. W., Sparks, F. T., Leutgeb, S. & Leutgeb, J. K. Hippocampal CA2 activity patterns change over time to a larger extent than between spatial contexts. *Neuron* **85**, 190-201, doi:10.1016/j.neuron.2014.12.001 (2015).

11 Magee, J. C. & Grienberger, C. Synaptic Plasticity Forms and Functions. *Annu Rev Neurosci*, doi:10.1146/annurev-neuro-090919-022842 (2020).

12 Buchanan, K. A. & Mellor, J. R. The activity requirements for spike timing-dependent plasticity in the hippocampus. *Front Synaptic Neurosci* **2**, 11, doi:10.3389/fnsyn.2010.00011 (2010).

13 Sheffield, M. E. & Dombeck, D. A. Calcium transient prevalence across the dendritic arbour predicts place field properties. *Nature* **517**, 200-204, doi:10.1038/nature13871 (2015).

14 Sheffield, M. E. & Dombeck, D. A. Dendritic mechanisms of hippocampal place field formation. *Curr Opin Neurobiol* **54**, 1-11, doi:10.1016/j.conb.2018.07.004 (2019).

15 Sheffield, M. E. J., Adoff, M. D. & Dombeck, D. A. Increased Prevalence of Calcium Transients across the Dendritic Arbor during Place Field Formation. *Neuron* **96**, 490-504 e495, doi:10.1016/j.neuron.2017.09.029 (2017).

16 Pedrosa, V. & Clopath, C. The interplay between somatic and dendritic inhibition promotes the emergence and stabilization of place fields. *PLoS Comput Biol* **16**, e1007955, doi:10.1371/journal.pcbi.1007955 (2020).

17 Freund, T. F. & Buzsaki, G. Interneurons of the hippocampus. *Hippocampus* **6**, 347-470, doi:10.1002/(SICI)1098-1063(1996)6:4<347::AID-HIPO1>3.0.CO;2-I (1996).

18 Hainmueller, T. & Bartos, M. Parallel emergence of stable and dynamic memory engrams in the hippocampus. *Nature* **558**, 292-296, doi:10.1038/s41586-018-0191-2 (2018).

19 Dupret, D., O'Neill, J., Pleydell-Bouverie, B. & Csicsvari, J. The reorganization and reactivation of hippocampal maps predict spatial memory performance. *Nat Neurosci* **13**, 995-1002, doi:10.1038/nn.2599 (2010).

20 Kentros, C. Hippocampal place cells: the "where" of episodic memory? *Hippocampus* **16**, 743-754, doi:10.1002/hipo.20199 (2006).

21 Kentros, C. G., Agnihotri, N. T., Streater, S., Hawkins, R. D. & Kandel, E. R. Increased attention to spatial context increases both place field stability and spatial memory. *Neuron* **42**, 283-295, doi:10.1016/s0896-6273(04)00192-8 (2004).

22 Robinson, N. T. M. *et al.* Targeted Activation of Hippocampal Place Cells Drives Memory-Guided Spatial Behavior. *Cell* **183**, 1586-1599 e1510, doi:10.1016/j.cell.2020.09.061 (2020).

23 Frank, L. M., Stanley, G. B. & Brown, E. N. Hippocampal plasticity across multiple days of exposure to novel environments. *J Neurosci* **24**, 7681-7689, doi:10.1523/JNEUROSCI.1958-04.2004 (2004).

24 Bittner, K. C., Milstein, A. D., Grienberger, C., Romani, S. & Magee, J. C. Behavioral time scale synaptic plasticity underlies CA1 place fields. *Science* **357**, 1033-1036, doi:10.1126/science.aan3846 (2017).

25 Cohen, J. D., Bolstad, M. & Lee, A. K. Experience-dependent shaping of hippocampal CA1 intracellular activity in novel and familiar environments. *Elife* **6**, doi:10.7554/eLife.23040 (2017).

26 Epsztein, J., Brecht, M. & Lee, A. K. Intracellular determinants of hippocampal CA1 place and silent cell activity in a novel environment. *Neuron* **70**, 109-120, doi:10.1016/j.neuron.2011.03.006 (2011).

27 Leutgeb, S., Leutgeb, J. K., Treves, A., Moser, M. B. & Moser, E. I. Distinct ensemble codes in hippocampal areas CA3 and CA1. *Science* **305**, 1295-1298, doi:10.1126/science.1100265 (2004).

28 Ziv, Y. *et al.* Long-term dynamics of CA1 hippocampal place codes. *Nat Neurosci* **16**, 264-266, doi:10.1038/nn.3329 (2013).

29 Geiller, T., Fattahi, M., Choi, J. S. & Royer, S. Place cells are more strongly tied to landmarks in deep than in superficial CA1. *Nat Commun* **8**, 14531, doi:10.1038/ncomms14531 (2017).

30 Lee, I., Rao, G. & Knierim, J. J. A double dissociation between hippocampal subfields: differential time course of CA3 and CA1 place cells for processing changed environments. *Neuron* **42**, 803-815, doi:10.1016/j.neuron.2004.05.010 (2004).
31 Roth, E. D., Yu, X., Rao, G. & Knierim, J. J. Functional differences in the backward shifts of CA1 and CA3 place fields in novel and familiar environments. *PLoS One* **7**, e36035, doi:10.1371/journal.pone.0036035 (2012).
32 Mehta, M. R., Quirk, M. C. & Wilson, M. A. Experience-dependent asymmetric shape of hippocampal receptive fields. *Neuron* **25**, 707-715, doi:10.1016/s0896-6273(00)81072-7 (2000).
33 Ekstrom, A. D., Meltzer, J., McNaughton, B. L. & Barnes, C. A. NMDA receptor antagonism blocks experience-dependent expansion of hippocampal "place fields". *Neuron* **31**, 631-638, doi:10.1016/s0896-6273(01)00401-9 (2001).
34 Reijmers, L. G., Perkins, B. L., Matsuo, N. & Mayford, M. Localization of a stable neural correlate of associative memory. *Science* **317**, 1230-1233, doi:10.1126/science.1143839 (2007).
35 Liu, X. *et al.* Optogenetic stimulation of a hippocampal engram activates fear memory recall. *Nature* **484**, 381-385, doi:10.1038/nature11028 (2012).
36 Kinsky, N. R., Sullivan, D. W., Mau, W., Hasselmo, M. E. & Eichenbaum, H. B. Hippocampal Place Fields Maintain a Coherent and Flexible Map across Long Timescales. *Curr Biol* **28**, 3578-3588 e3576, doi:10.1016/j.cub.2018.09.037 (2018).
37 Rubin, A., Geva, N., Sheintuch, L. & Ziv, Y. Hippocampal ensemble dynamics timestamp events in long-term memory. *Elife* **4**, doi:10.7554/eLife.12247 (2015).
38 Jeantet, Y. & Cho, Y. H. Evolution of hippocampal spatial representation over time in mice. *Neurobiol Learn Mem* **98**, 354-360, doi:10.1016/j.nlm.2012.10.004 (2012).
39 Mankin, E. A. *et al.* Neuronal code for extended time in the hippocampus. *Proc Natl Acad Sci U S A* **109**, 19462-19467, doi:10.1073/pnas.1214107109 (2012).
40 Nakazawa, K. *et al.* Requirement for hippocampal CA3 NMDA receptors in associative memory recall. *Science* **297**, 211-218, doi:10.1126/science.1071795 (2002).
41 Colgin, L. L., Moser, E. I. & Moser, M. B. Understanding memory through hippocampal remapping. *Trends Neurosci* **31**, 469-477, doi:10.1016/j.tins.2008.06.008 (2008).
42 Muller, R. U. & Kubie, J. L. The effects of changes in the environment on the spatial firing of hippocampal complex-spike cells. *J Neurosci* **7**, 1951-1968 (1987).
43 Bostock, E., Muller, R. U. & Kubie, J. L. Experience-dependent modifications of hippocampal place cell firing. *Hippocampus* **1**, 193-205, doi:10.1002/hipo.450010207 (1991).
44 Fyhn, M., Hafting, T., Treves, A., Moser, M. B. & Moser, E. I. Hippocampal remapping and grid realignment in entorhinal cortex. *Nature* **446**, 190-194, doi:10.1038/nature05601 (2007).
45 Mehta, M. R., Barnes, C. A. & McNaughton, B. L. Experience-dependent, asymmetric expansion of hippocampal place fields. *Proc Natl Acad Sci U S A* **94**, 8918-8921, doi:10.1073/pnas.94.16.8918 (1997).
46 Dombeck, D. A., Harvey, C. D., Tian, L., Looger, L. L. & Tank, D. W. Functional imaging of hippocampal place cells at cellular resolution during virtual navigation. *Nat Neurosci* **13**, 1433-1440, doi:10.1038/nn.2648 (2010).

47 McNamara, C. G., Tejero-Cantero, A., Trouche, S., Campo-Urriza, N. & Dupret, D. Dopaminergic neurons promote hippocampal reactivation and spatial memory persistence. *Nat Neurosci* **17**, 1658-1660, doi:10.1038/nn.3843 (2014).

48 Davoudi, H. & Foster, D. J. Acute silencing of hippocampal CA3 reveals a dominant role in place field responses. *Nat Neurosci* **22**, 337-342, doi:10.1038/s41593-018-0321-z (2019).

49 Hunsaker, M. R., Rosenberg, J. S. & Kesner, R. P. The role of the dentate gyrus, CA3a,b, and CA3c for detecting spatial and environmental novelty. *Hippocampus* **18**, 1064-1073, doi:10.1002/hipo.20464 (2008).

50 Dolleman-van der Weel, M. J. *et al.* The nucleus reuniens of the thalamus sits at the nexus of a hippocampus and medial prefrontal cortex circuit enabling memory and behavior. *Learn Mem* **26**, 191-205, doi:10.1101/lm.048389.118 (2019).

51 Nitz, D. & McNaughton, B. Differential modulation of CA1 and dentate gyrus interneurons during exploration of novel environments. *J Neurophysiol* **91**, 863-872, doi:10.1152/jn.00614.2003 (2004).

52 Yu, X., Knierim, J. J., Lee, I. & Shouval, H. Z. Simulating place field dynamics using spike timing-dependent plasticity. *Neurocomputing* **69**, 1253-1259 (2006).

53 Lisman, J. & Spruston, N. Questions about STDP as a General Model of Synaptic Plasticity. *Front Synaptic Neurosci* **2**, 140, doi:10.3389/fnsyn.2010.00140 (2010).

54 Graupner, M., Wallisch, P. & Ostojic, S. Natural Firing Patterns Imply Low Sensitivity of Synaptic Plasticity to Spike Timing Compared with Firing Rate. *J Neurosci* **36**, 11238-11258, doi:10.1523/JNEUROSCI.0104-16.2016 (2016).

55 Hussaini, S. A., Kempadoo, K. A., Thuault, S. J., Siegelbaum, S. A. & Kandel, E. R. Increased size and stability of CA1 and CA3 place fields in HCN1 knockout mice. *Neuron* **72**, 643-653, doi:10.1016/j.neuron.2011.09.007 (2011).

56 Bittner, K. C. *et al.* Conjunctive input processing drives feature selectivity in hippocampal CA1 neurons. *Nat Neurosci* **18**, 1133-1142, doi:10.1038/nn.4062 (2015).

57 Fattahi, M., Sharif, F., Geiller, T. & Royer, S. Differential Representation of Landmark and Self-Motion Information along the CA1 Radial Axis: Self-Motion Generated Place Fields Shift toward Landmarks during Septal Inactivation. *J Neurosci* **38**, 6766-6778, doi:10.1523/JNEUROSCI.3211-17.2018 (2018).

58 Thompson, L. T. & Best, P. J. Long-term stability of the place-field activity of single units recorded from the dorsal hippocampus of freely behaving rats. *Brain Res* **509**, 299-308, doi:10.1016/0006-8993(90)90555-p (1990).

59 Wood, E. R., Dudchenko, P. A., Robitsek, R. J. & Eichenbaum, H. Hippocampal neurons encode information about different types of memory episodes occurring in the same location. *Neuron* **27**, 623-633, doi:10.1016/s0896-6273(00)00071-4 (2000).

60 Krishnan, S., Cherian, C. & Sheffield, M. E. J. Changing reward expectation transforms spatial encoding and retrieval in the hippocampus. *bioRxiv*, 2020.2009.2013.295469, doi:10.1101/2020.09.13.295469 (2020).

61 Anderson, M. I. & Jeffery, K. J. Heterogeneous modulation of place cell firing by changes in context. *J Neurosci* **23**, 8827-8835 (2003).

62 Hasselmo, M. E. & Eichenbaum, H. Hippocampal mechanisms for the context-dependent retrieval of episodes. *Neural Netw* **18**, 1172-1190, doi:10.1016/j.neunet.2005.08.007 (2005).
63 Cai, D. J. *et al.* A shared neural ensemble links distinct contextual memories encoded close in time. *Nature* **534**, 115-118, doi:10.1038/nature17955 (2016).
64 Allegra, M., Posani, L., Gomez-Ocadiz, R. & Schmidt-Hieber, C. Differential Relation between Neuronal and Behavioral Discrimination during Hippocampal Memory Encoding. *Neuron* **108**, 1103-1112 e1106, doi:10.1016/j.neuron.2020.09.032 (2020).
65 Madar, A. *Pattern Separation in the Hippocampus, in Health and Epilepsy* PhD thesis, University of Wisconsin-Madison, (2018).
66 Bourboulou, R. *et al.* Dynamic control of hippocampal spatial coding resolution by local visual cues. *Elife* **8**, doi:10.7554/eLife.44487 (2019).
67 Lee, S. W., O'Doherty, J. P. & Shimojo, S. Neural computations mediating one-shot learning in the human brain. *PLoS Biol* **13**, e1002137, doi:10.1371/journal.pbio.1002137 (2015).
68 Stachenfeld, K. L., Botvinick, M. M. & Gershman, S. J. The hippocampus as a predictive map. *Nat Neurosci* **20**, 1643-1653, doi:10.1038/nn.4650 (2017).
69 Abbott, L. F. & Blum, K. I. Functional significance of long-term potentiation for sequence learning and prediction. *Cereb Cortex* **6**, 406-416, doi:10.1093/cercor/6.3.406 (1996).
70 Clewett, D., DuBrow, S. & Davachi, L. Transcending time in the brain: How event memories are constructed from experience. *Hippocampus* **29**, 162-183, doi:10.1002/hipo.23074 (2019).
71 Heys, J. G., Rangarajan, K. V. & Dombeck, D. A. The functional micro-organization of grid cells revealed by cellular-resolution imaging. *Neuron* **84**, 1079-1090, doi:10.1016/j.neuron.2014.10.048 (2014).
72 Aronov, D., Nevers, R. & Tank, D. W. Mapping of a non-spatial dimension by the hippocampal-entorhinal circuit. *Nature* **543**, 719-722, doi:10.1038/nature21692 (2017).
73 Mukamel, E. A., Nimmerjahn, A. & Schnitzer, M. J. Automated analysis of cellular signals from large-scale calcium imaging data. *Neuron* **63**, 747-760, doi:10.1016/j.neuron.2009.08.009 (2009).
74 Tampuu, A., Matiisen, T., Olafsdottir, H. F., Barry, C. & Vicente, R. Efficient neural decoding of self-location with a deep recurrent network. *PLoS Comput Biol* **15**, e1006822, doi:10.1371/journal.pcbi.1006822 (2019).
75 Ho, J., Tumkaya, T., Aryal, S., Choi, H. & Claridge-Chang, A. Moving beyond P values: data analysis with estimation graphics. *Nat Methods* **16**, 565-566, doi:10.1038/s41592-019-0470-3 (2019).
76 Dragoi, G. & Tonegawa, S. Preplay of future place cell sequences by hippocampal cellular assemblies. *Nature* **469**, 397-401, doi:10.1038/nature09633 (2011).
77 Madar, A. D., Ewell, L. A. & Jones, M. V. Pattern separation of spiketrains in hippocampal neurons. *Sci Rep* **9**, 5282, doi:10.1038/s41598-019-41503-8 (2019).
78 Glaser, J. I. *et al.* Machine learning for neural decoding. arXiv:1708.00909 (2017). <https://ui.adsabs.harvard.edu/abs/2017arXiv170800909G>.
79 Hochreiter, S. & Schmidhuber, J. Long short-term memory. *Neural Comput* **9**, 1735-1780, doi:10.1162/neco.1997.9.8.1735 (1997).

621

622

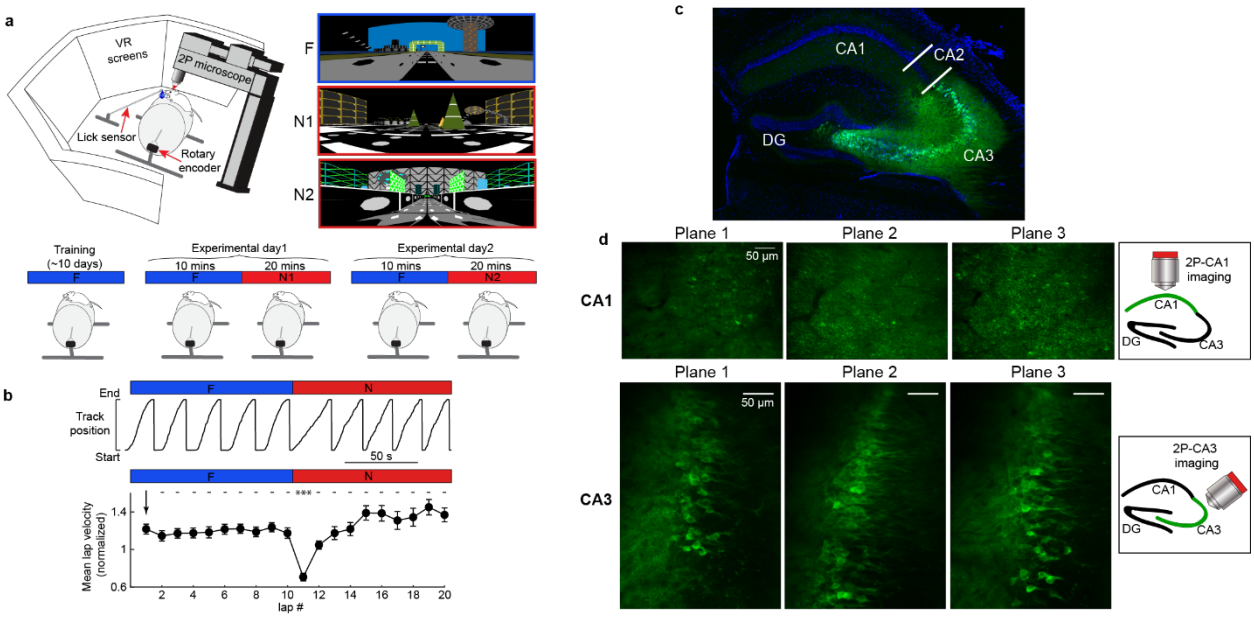

Fig. 1: Experimental set up.

a, Top left, depiction of the virtual reality (VR) set up. Top right, the familiar (F) and two novel (N1 and N2) environments. Bottom: Scheme of the experimental procedure. **b,** Top: Single mouse behavior showing track position versus time during an F to N switch. Bottom: Summary data across all mice of mean lap velocity during F and N (n = 20 sessions in 11 mice). Lap velocity is normalized to the mean lap velocity in each mouse ± SEM, and each lap is compared to the first lap in F using a one-way ANOVA with Tukey HSD post hoc test. ***, $P < 0.001$. **c,** Brain slice showing specific CA3 expression of cre-dependent GCaMP6f (green) and DAPI for nuclei (blue) from a Grik4-cre transgenic mouse. **d,** Example field of views (FOV) from multiplane imaging in CA1 (top) and CA3 (bottom). Right: scheme of the position for the objective during imaging.

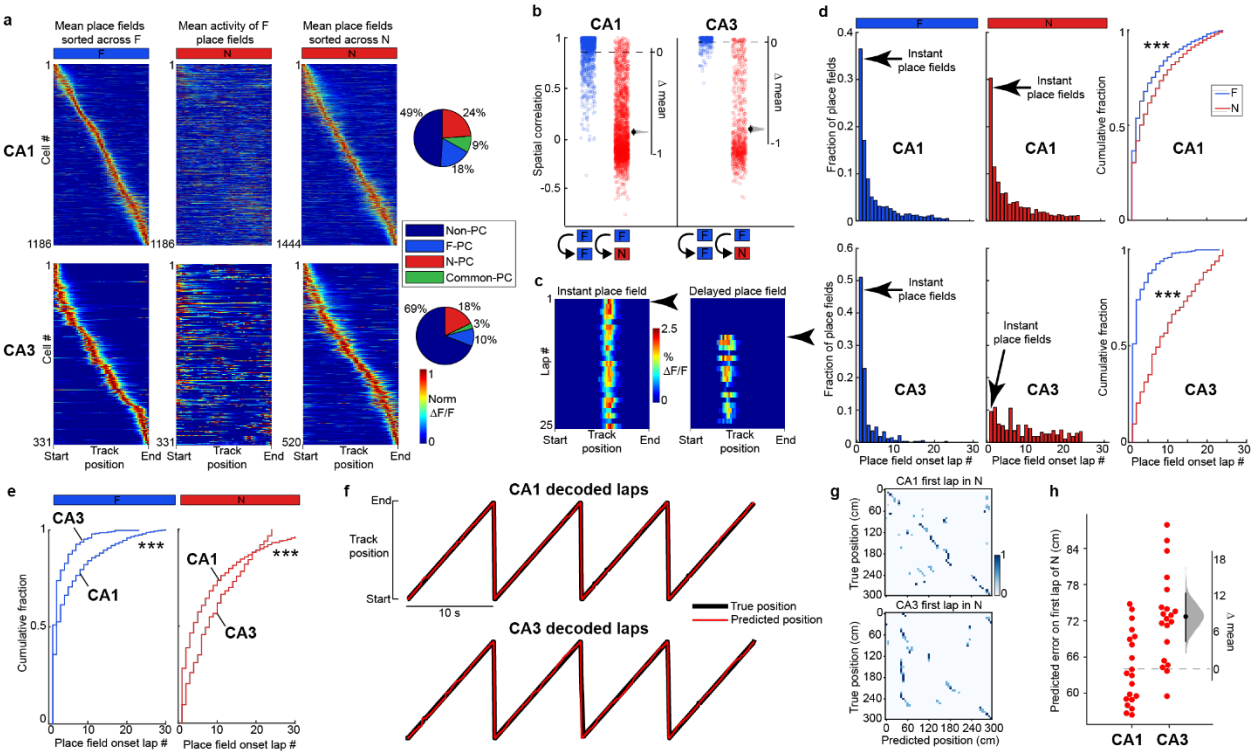

Fig. 2: Place field emergence in novel environments is rapid in CA1 but gradual in CA3

a, Left: mean place fields (PFs) in F sorted by track position. Middle: mean activity of the same neurons on the left in N. Right: mean place fields in N sorted by track position. Far right: Percentage of place cells in F and N or common to both from all active neurons. CA1, top panels; CA3, bottom panels. ΔF/F activity is normalized to each neurons' maximum transient amplitude. *n* = 7 sessions in 4 mice for CA1, *n* = 13 sessions in 7 mice for CA3. Only place cells with single PFs are displayed, but place cells with multiple PFs are included in the pie charts and later analyses. **b,** Pearson's correlation coefficient of each cell's average activity map within F (blue, CA1 *n* = 1392, CA3 *n* = 320 neurons with activity in both halves of the F session) and between F and N (red, CA1 *n* = 2283, CA3 *n* = 698 neurons with activity in both sessions and a PF in one of them). Bootstrapped mean difference (Δ) with distribution of the mean (gray) and

95% confidence interval (error bar) on the right of each plot (see Methods). **c,** Example of an instant PF (left) and delayed PF (right) in N. Arrows indicate PF onset lap. **d,** Histograms of PF onset laps in F (left, CA1 n = 1643 PFs, CA3 n = 336 PFs) and N (middle, CA1 n = 1712 PFs, CA3 n = 532 PFs) and cumulative fraction plots for F and N (right). Wilcoxon rank sum test. ***, $P < 0.001$. **e,** Cumulative fraction plots for CA1 and CA3 PF onset lap in F (left) and in N (right). Wilcoxon rank sum test. ***, $P < 0.001$. **f,** Example mouse showing true track position (black) on laps 37-40 and the predicted position (red) decoded by an LSTM decoder (see Methods). CA1, top; CA3, bottom. **g,** Confusion matrix between the predicted (x-axis) and the true (y-axis) position for the first lap in N. **h,** Predicted error on the first lap in N for CA1 and CA3. Each dot represents the decoding error for one decoder trial built based on the activity of 200 randomly chosen place cells from CA1 (left) or CA3 (right). n = 20 decoder trials. Bootstrapped mean difference (Δ) with 95% CI (error bar) on the right.

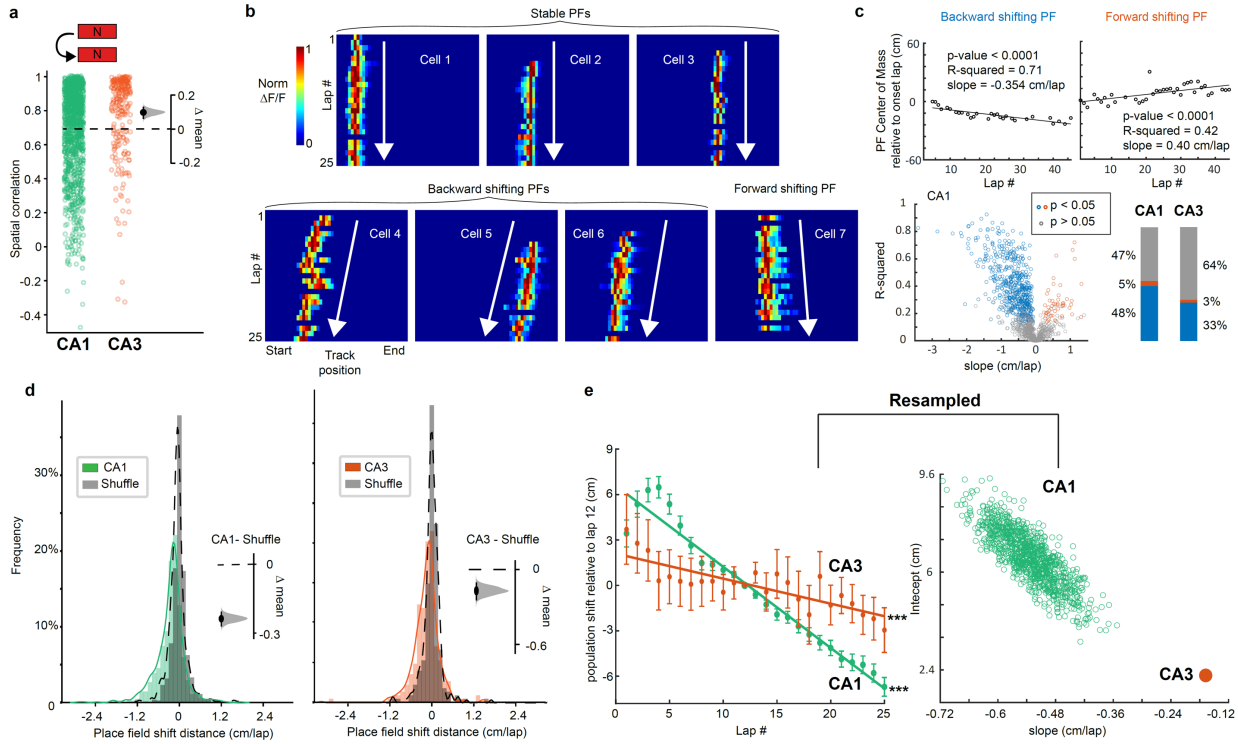

Fig. 3: CA3 place fields exhibit relative lap-by-lap stability while CA1 place fields shift with experience in novel environments

a, Pearson's correlation coefficient of all neurons with place fields within N (average activity map in first 10 laps versus next 10 laps of session: CA1 *n* = 1238, CA3 *n* = 255 neurons). Bootstrapped mean difference (Δ) between CA1 and CA3 shown on the right. **b,** Example place cells with stable or shifting place fields (PFs) in N (lap-by-lap activity for the first 25 laps). White arrows depict the direction of shifting. **c,** Linear regression analysis on the center of mass (COM) of individual PFs (CA1 in N) shows a high number of significantly shifting PFs (blue and red dots and bars). The slope measures the direction and amplitude of the PF shift: for significantly shifting PFs, backward is blue, forward is red. CA3 has a lower proportion of significantly shifting PFs than CA1. **d,** Histograms of the COM difference between last and onset

674 laps (5-lap weighted average, see Methods) normalized by the number of laps for each PFs in N
675 for CA1 and CA3. Shuffling the lap numbers (grey distributions) reveals an overrepresentation
676 of backward shifting PFs, as confirmed by the bootstrapped mean difference (Δ, insets). **e,** Left,
677 Mean ± SEM, over all PFs, of 5-lap sliding average COM difference relative to lap 12 (see
678 Methods), in N. CA1 (green) and CA3 (orange). Linear regression analysis (on all data points, not
679 means) shows that the population of PFs shifts backwards significantly, both in CA1 and CA3.
680 ***, $P < 0.001$. Right, The CA1 dataset was resampled 1000x using $n = 175$ PFs to match the
681 number of CA3 PFs and the slope and intercept of the regression line was measured each time
682 (green dots). CA1 slopes are always steeper than the CA3 slope indicating that the CA1
683 population shifts significantly faster than CA3.
684

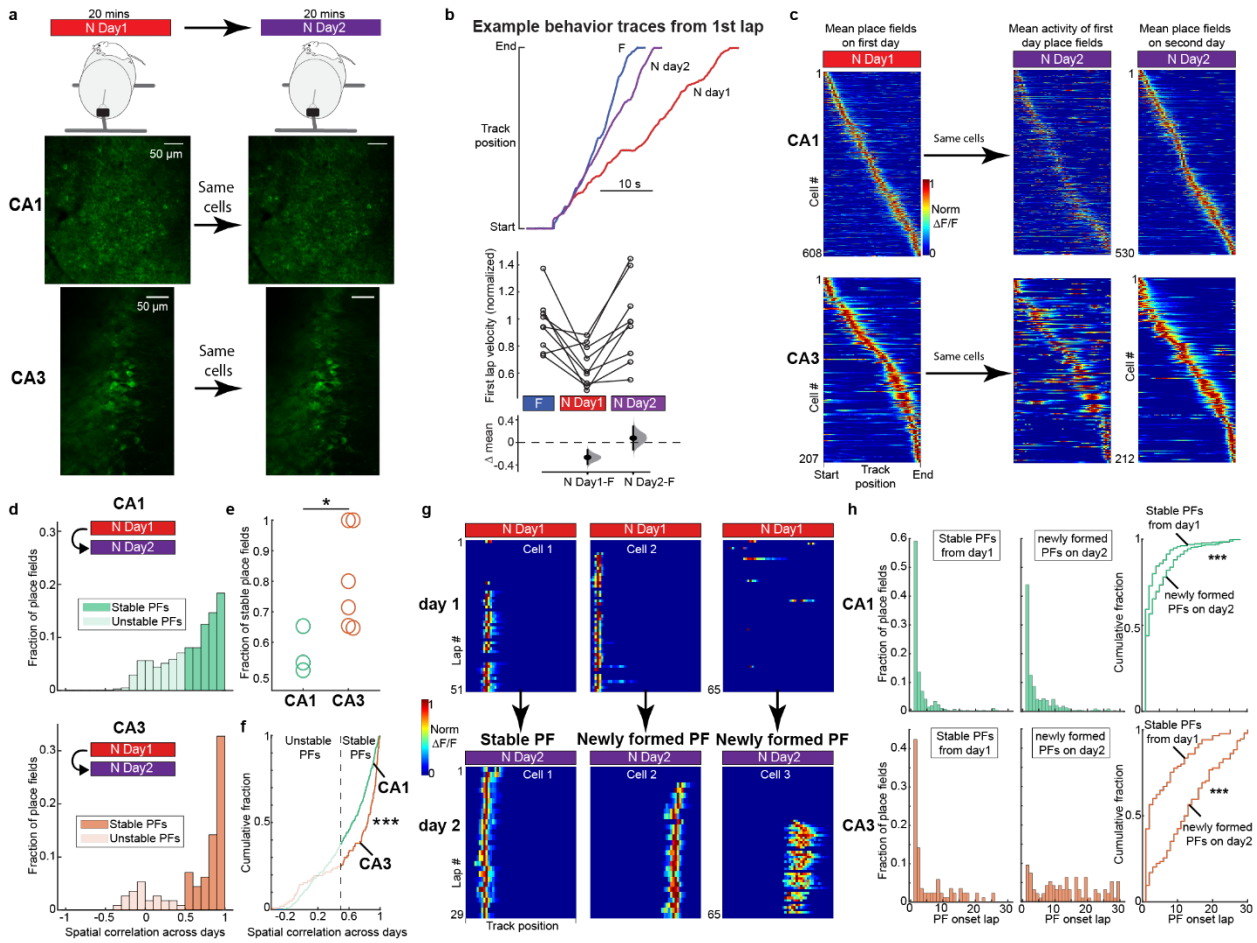

Fig. 4: CA3 place fields exhibit higher stability across days than CA1 place fields and rapidly reappear upon re-exposure to the environment

a, Experimental setup. Top: mice are recorded for 20 min in N across 2 days. Bottom: example field of view from one imaging plane from CA1 and CA3 across 2 days showing the same cells. scale bar = 50 µm. **b,** Top, example mouse behavior showing track position for the first lap in F (blue), N day 1 (red) and N day 2 (purple). Bottom, summary across all mice of first lap velocity in F, N day1 and N day2. Lap velocities were normalized to the mean velocity in F in each mouse (n = 11 mice). Bootstrapped mean difference (Δ) between F and N day 1, and F and N day 2. Note that lap velocity is only different on N day 1. **c,** Left: mean place fields in N on day 1 sorted by track position. Middle: mean activity of the same neurons on the left on day 2 in N. Right:

696 mean place fields in N on day 2 sorted by track position. **d,** Histograms of Pearson's correlation
697 coefficient of average activity map across days in N. Spatial correlations greater than 0.5 were
698 considered stable place fields and less than 0.5 unstable. CA1 n = 409, CA3 n = 113 neurons with
699 PFs in both sessions. **e,** Fraction of stable place fields across days per mouse in CA1 and CA3.
700 Wilcoxon rank sum test. *P < 0.05. **f,** Cumulative fraction plots of Pearson's correlation
701 coefficient in N across days in CA1 and CA3 from the same data shown in (**c**). Wilcoxon rank
702 sum test. ***, P < 0.001. **g,** Example of a stable place field (left), an unstable place field with a
703 newly formed place field on day 2 (middle) and a newly formed place field on day 2 (right).
704 Place field transients shown lap-by-lap for all laps in N on day 1 and day 2 from the same 3 cells.
705 **h,** Histograms of place field onset laps in N on day 2 for stable place fields (left), and newly
706 formed place fields (middle) in CA1 (top) and CA3 (bottom). Right: cumulative fraction plots of
707 histogram data. Wilcoxon rank sum test. ***, P < 0.001. CA1 stable n = 251 PFs, newly formed,
708 n = 333 PFs, CA3 stable n = 72 PFs, newly formed, n = 94 PFs.
709

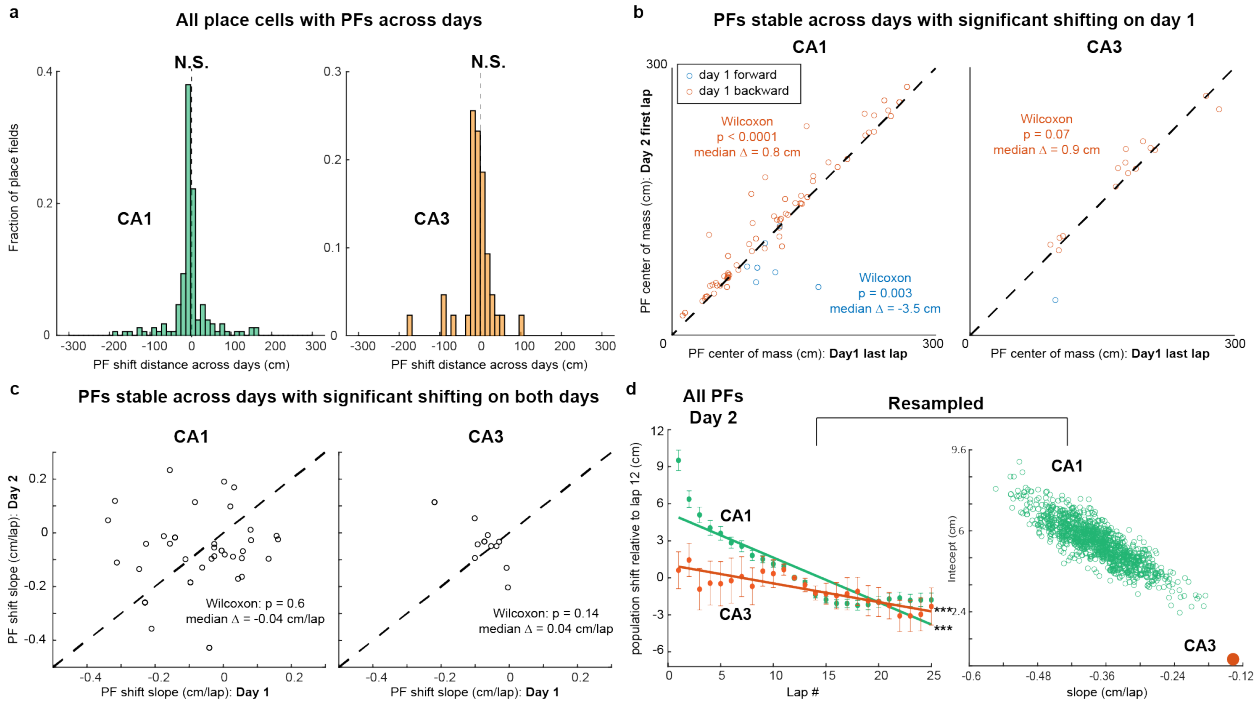

Fig. 5: Place field shifting resets and continues upon first re-exposure to N on day 2.

a, Histogram of place field (PF) shifts across days for CA1 (left, n =171 PFs) and CA3 (right, n = 43 PFs). The shifts were calculated as the difference between each PF's center of mass (COM) of the last active lap on day 1 and first active lap in day 2. Only place cells with PFs on both days are included. Wilcoxon signed rank test, N.S., $P > 0.05$. **b,** Comparison of COM position at the end of day 1 and COM position at the start of day 2 for PFs with day-to-day correlation > 0.5 and significant shifting on day 1 (see Fig. 3c). Dashed diagonal: identity line. On day 2, PFs tend to reset towards the direction opposite of shifting on day 1. Wilcoxon sign-rank test on Day 2-Day 1 difference from 0 for backward and forward shifting (*P*-values and median in panel). **c,** Comparison of PF shifting slope on both days. No clear correlation is observed, but the Day 2-Day 1 difference is not significantly different from 0 (Wilcoxon sign-rank: *P*-values and medians in panel) and individual PF shifting was slow (close to 0 cm/lap) on both days. **d,** Same as Fig. 3e but for N day 2, using all PFs recorded that day. CA1 (green; *n* = 371 PFs from 3 mice) and

CA3 (orange; *n* = 84 PFs from 6 mice). The resampling analysis (1000 random resamples matching the CA3 sample size) shows that CA1 slopes are always steeper than the CA3 slope, indicating that on day 2 the CA1 population shifts backward faster than CA3.

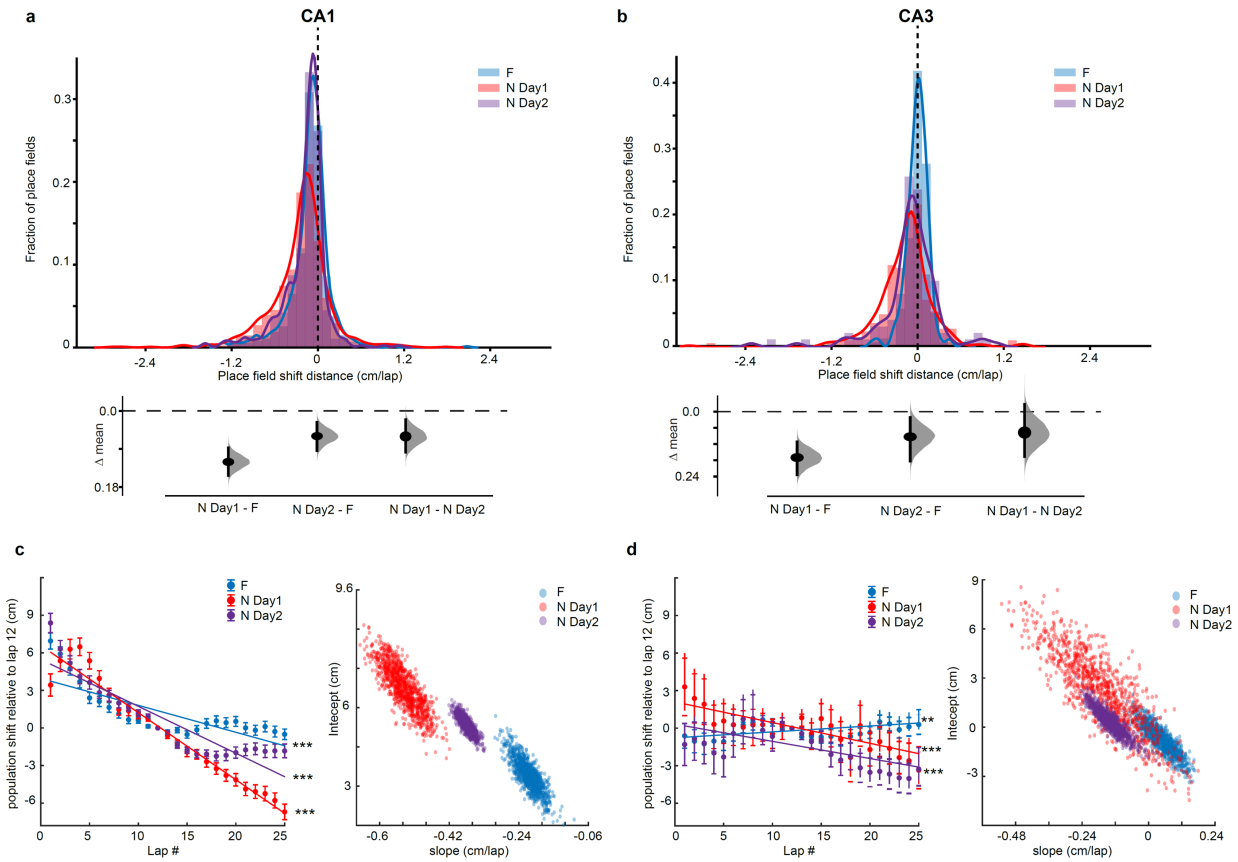

728

729 **Fig. 6: Population backward shifting slows down with familiarization across days**

730 **a,** Top, histograms of COM_{last_lap}-COM_{onset_lap} (session shift defined as in Fig. 3d) in Familiar (F), N

731 day 1 and N day 2, for CA1. Bottom, Bootstrapped mean difference (Δ) between the three

732 conditions. **b,** Same as a for CA3. **c,** Left, Same as Fig. 3e, comparing CA1 population shifts in F

733 (blue), N day 1 (red) and N day 2 (purple). ***, $P < 0.001$. The resampling analysis uses a

734 number of PFs equal to 80 percent of the number of PFs in the condition with lowest number of

735 PFs (1000 resamples). The lack of distribution overlap between conditions indicates dynamics

736 are significantly different. **d,** Same as c for CA3. Overlap in the slope distributions suggests that

737 population dynamics are similarly flat (slopes close to 0) although CA3 PFs shifting become

738 more homogeneous (smaller variance) with familiarization.